Electronic Supplementary Information (ESI)

Non-volatile organic field-effect transistor memory comprising sequestered metal nanoparticles in a diblock copolymer film

Chia-Min Chen,[†] Chih-Ming Liu,[†] Kung-Hwa Wei*[†] U-Ser Jeng,[‡] and Chiu-Hun Su[‡]

[†] Department of Materials Science and Engineering, National Chiao Tung University,

Hsinchu 30049, Taiwan; [‡]National Synchrotron Radiation Research Center,

101 Hsin-Ann Road, Science-Based Industrial Park,

Hsinchu 30077, Taiwan

E-mail: khwei@mail.nctu.edu.tw
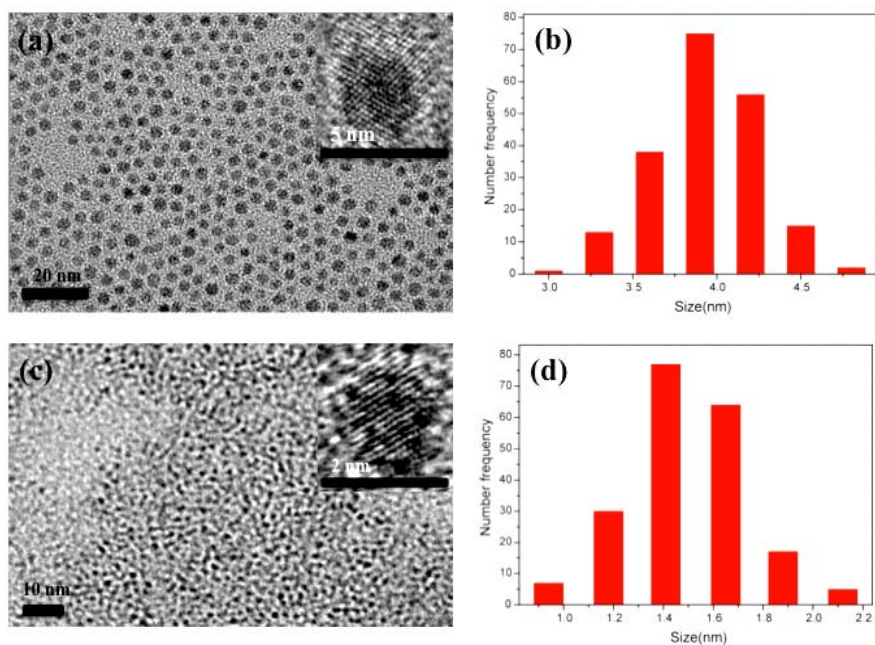
Figure S1. TEM images of the (a) DT-Ag and (c) Py-Pt NPs (dark spots), with corresponding size distributions presented in (b) and (d). Insets to (a) and (c): HRTEM images of the respective NPs.
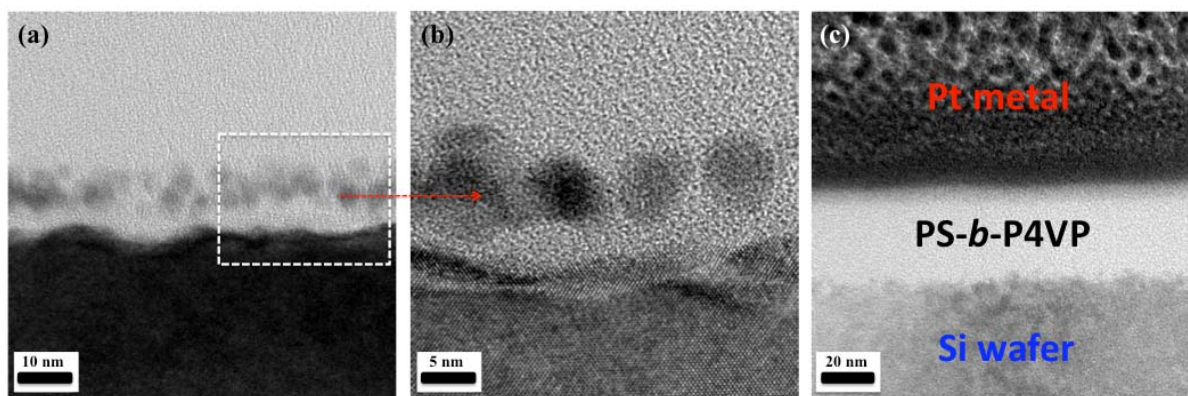
Figure S2. (a) Cross-sectional TEM images of a monolayer of the (DT-Ag$_{0.8}$@PS)-*b*-(Py-Pt$_{1.0}$@P4VP) micelles. The grey spheres having an average diameter of ca. 4 nm are the Ag NPs; they are located directly above the dark substrate. (b) Detailed view of the square zone marked in (a). (c) Cross-sectional TEM image of the neat PS-*b*-P4VP film, contrasted by the deposited Pt layer above and the Si substrate below; its thickness (ca. 30 nm) corresponds to a micelle monolayer (cf. Figure 2).
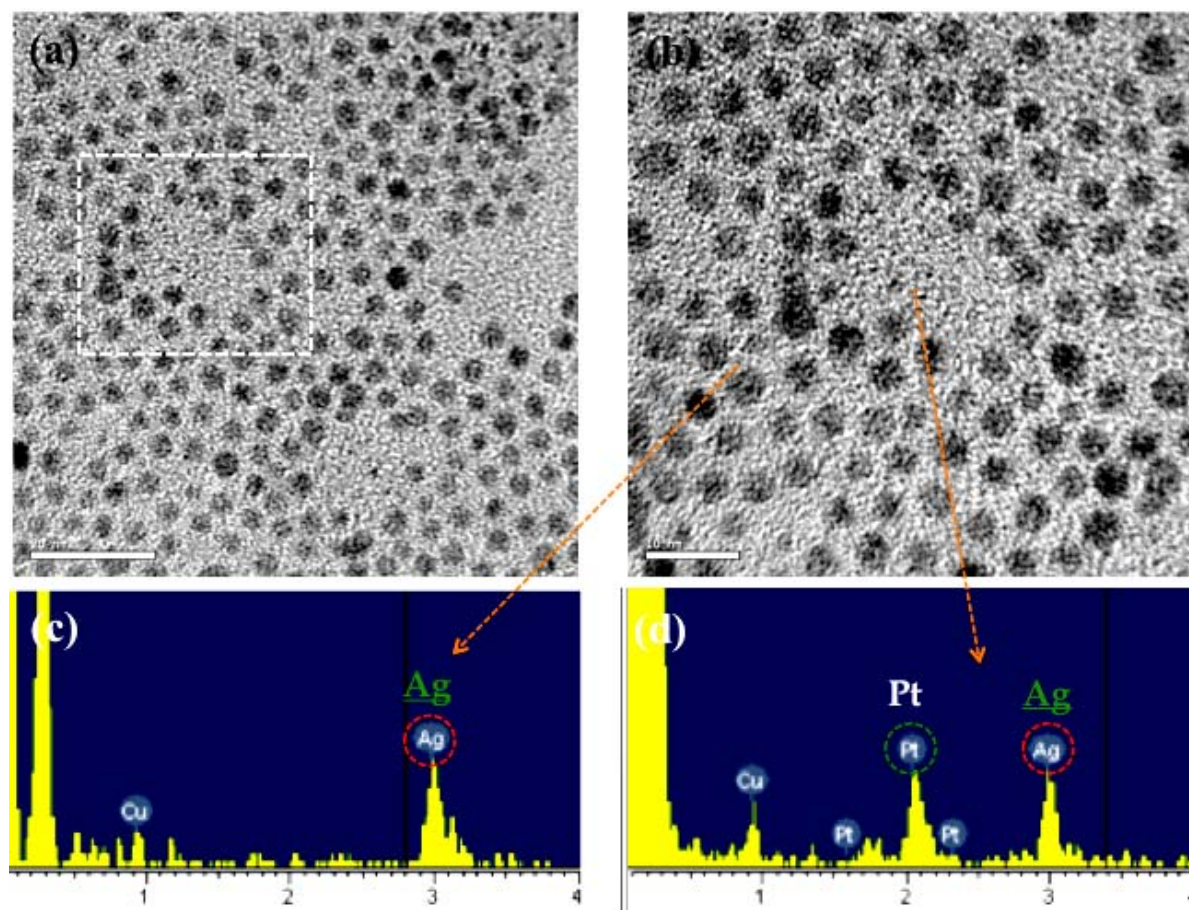
Figure S3. (a) TEM image of the (DT-Ag$_{1.0}$@PS)-*b*-(Py-Pt$_{1.0}$@P4VP) composite drop-casted onto a Cu net. (b) Expanded view of the squared zone in (a), highlighting a Py-Pt@P4VP core and its surroundings. (c, d) EDX spectra recorded from the respective zones of the Ag NPs (in the PS phase) and the Pt NPs (in the P4VP phase) within the NP/copolymer composite. Because the electron beam was wider than the dimensions of the Py-Pt@P4VP core, signals for both Ag and Pt elements appear in (d).

Thermal Stability. Figure S4 presents temperature-dependent GISAXS data for the composite film (DT-Ag$_{1.0}$@PS)-*b*-(Py-Pt$_{1.0}$@P4VP). The shoulder peak at a value of q_x of 0.0031 Å^{-1}, signifying the first hexagonal packing peak of the micelle cores, remained present upon elevating the temperature from 50 to 250 °C, indicating overall thermal stability. In contrast, the scattering peak at a value of q_x of 0.115 Å^{-1}, representing short-range ordering of the DT-Ag NPs, deteriorated when the temperature approached the value of T_g (ca. 100 °C) of PS,[S1,S2] and disappeared at temperatures above 100 °C. Subsequently, the scattering intensity in the q_x region 0.02–0.1 Å^{-1} gradually enhanced at temperatures above 125 °C and became saturated at 175 °C. We attribute this increased intensity at elevated temperatures to minor aggregation of the DT-Ag NPs, resulting from the greater mobility of the PS chains and the partial loss of the DT-Ag ligands. The loss of the ligands of the DT-Ag NPs was revealed through thermogravimetric analysis (TGA, Figure S4b).

Modeling the DT-Ag NPs in the form of polydisperse spheres with the Schultz distribution (Figure S5, Supporting Information)[S3,S4] allowed us to reasonably fit the GISAXS data in the higher-q_x region (Figure S4a), where the NPs dominated the scattering contribution.[S2,S5] The fitted mean particle sizes (with ca. 20% polydispersity in general), summarized in the inset to Figure S4b, indicate that the DT-Ag NPs having a diameter of ca. 3.9 nm aggregated to a size of 7.7 nm at 175 °C. The aggregation size changed little upon further elevation of the temperature from 175 to 250 °C; in this temperature range, however, we observed a continuous loss of ligands (Figure S4b). We speculate that the surrounding PS chains restricted the aggregation of the DT-Ag NPs to local regions after ligand depletion at temperatures near 250 °C. Had these DT-Ag NPs segregated out from the PS phase, ligand-depleted Ag NPs would have aggregated severely (for large, irregular aggregates) at high temperatures.

NP Trapping Strategy. To better understand the NP trapping mechanism, we synthesized Ag NPs passivated with alkanethiols having carbon chain lengths of 6, 8, 14, and 16 atoms, respectively; each of them (having the same Ag core size) entered the PS phase of the copolymer in the same manner as did the DT-Ag (C_{12}) NPs (Figure S6, Supporting Information). On the other hand, the same DT-Ag NPs surrounded, rather than being sequestered into, the PS corona phase, when we reduced the PS volume fraction (f_{PS}) of the copolymer from 0.88 for PS_{56k}-b-$P4VP_{8k}$ having a spherical micelle morphology (Figure 2a) to 0.71 for PS_{48k}-b-$P4VP_{21k}$ having a cylindrical micelle morphology (Figure S7a).[S3] These results indicate that the spherical morphology of the neat diblock copolymer, rather than the alkanethiol chain length of the passivated Ag NPs, played a more decisive role in the successful embedding of the alkanethiol-passivated Ag NPs into the PS phase.

In the presence of the DT-Ag NPs, the spherical micelles of the diblock copolymer PS_{48k}-b-$P4VP_{21k}$ in solution were, however, retained after solvent evaporation (Figure S7b). It is likely that the spherical micelle morphology observed for the composite DT-$Ag_{1.0}$/PS_{48k}-b-$P4VP_{21k}$, similar to those observed in previous reports,[S6,S7] was kinetically stabilized by the alkanethiol-passivated metal NPs that segregated to the outer edges of the PS corona phase during solvent evaporation. Presumably, these alkanethiol-passivated metal NPs with short alkyl chains were driven by higher conformational entropy to the outer edges to alleviate the PS chain stretching, thereby suppressing the spherical-to-cylindrical micelle transition of the diblock copolymer PS_{48k}-b-$P4VP_{21k}$ having a value of f_{PS} of 0.71 during solvent evaporation. An analogy may be the locking of the phase transformation in sphere-forming A-b-B/A blends: The existence of the corresponding homopolymer in the matrix phase for micelles alleviates the packing frustration of the coronal blocks forming the matrix phase, whereby the coronal chains that otherwise must stretch far to reach the vertexes of the Wigner–Seitz cell can relax upon localization of the homopolymers near the vertexes.[S8]

Based on all the structural information obtained, we suggest the following scenario to explain the successful embedding of the alkanethiol-passivated DT-Ag NPs in the PS phase. In our designated mixing process using toluene, which is selective for PS and the DT-Ag NPs, the alkanethiol-passivated metal NPs could mix well within the PS corona phase of the highly asymmetric PS_{56k}-b-(Py-Pt@$P4VP_{8k}$) having a spherical micelle morphology at thermal equilibrium. Upon solvent evaporation in the subsequent film casting process, the DT-Ag NPs thereby resided stably within the PS phase of the spherical micelles of the diblock copolymer, leading to hierarchically ordered composite films. Prepared with the modified one-phase synthesis, which reduces the salt contamination and provides decent polydispersity (ca. 20%), the DT-Ag and Py-Pt NPs were appropriate materials for solution mixing in toluene (i.e., little precipitation or aggregation of the NPs occurred).
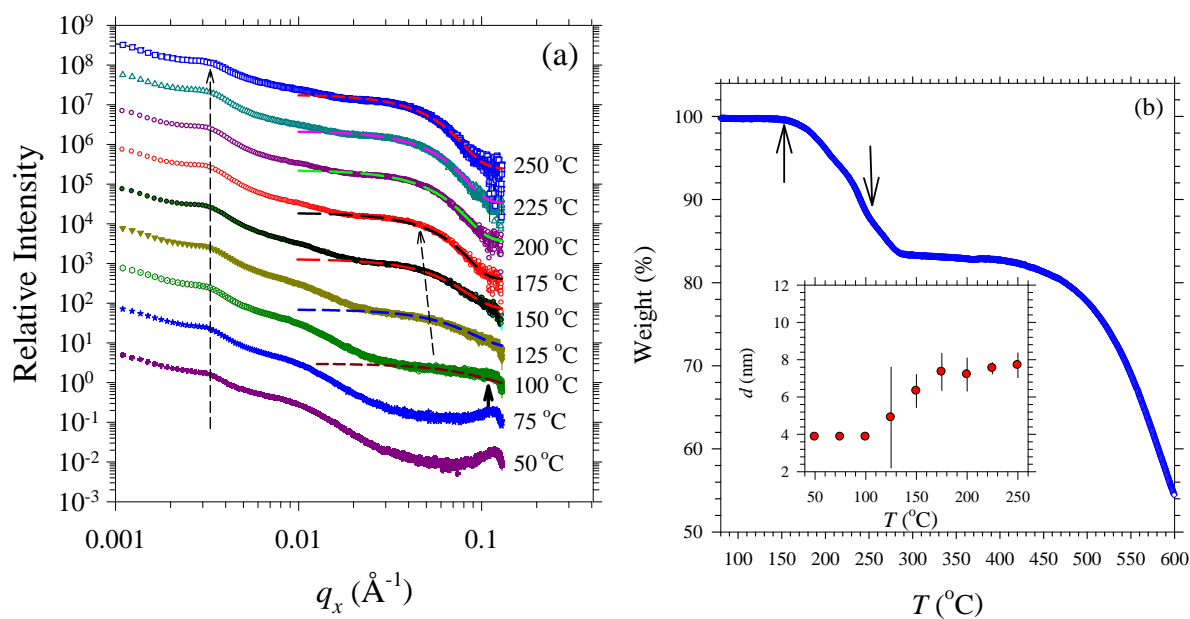
Figure S4. (a) Temperature-dependent GISAXS data, with rescaled intensity for clarity, for the composite (DT-Ag$_{1.0}$@PS)-b-(Py-Pt$_{1.0}$@P4VP). In the higher-q_x region, each set of data was fitted (dashed curves) using a model of polydisperse spheres; the fitted values for the mean diameter (d) are provided in the inset to (b). The dotted line at $q_x = 0.0031$ Å^{-1} indicates the constant first-order peak of hexagonal packing; the short arrow at $q_x = 0.115$ Å^{-1} marks the melting of the peak of the ordered DT-Ag NPs at temperatures near 100 °C. (b) TGA data revealing a total weight loss of ca. 17% from the DT-Ag NPs at temperatures between 150 and 280 °C, resulting from the loss of ligands.

Using the sphere form factor $P(q,r) = |F(q,r)^2| \propto (3j_1(qr)/qr)|^2$ and a Schultz function for size distribution, with the first-order spherical Bessel function j_1 and the wavevector transfer $q = 4\pi\lambda^{-1}\sin\theta$ (defined by the scattering angle 2θ and the wavelength λ of the X-rays), we fit the GISAXS intensity distribution with

$$I(q) = \sum_i n_p(r_i)P(q,r_i) = <n_p> \int P(q,r)f(r)dr = <n_p><P(q)>. \tag{1}$$

Here, $n_p(r) = <n_p>f(r)$ is the number density of the particles of size r, with $<n_p>$ being the mean number density and $f(r)$ being the Schultz distribution:

$$f(r) = \left(\frac{z+1}{r_a}\right)^{z+1} r^z \exp\left[-\left(\frac{z+1}{r_a}\right)r\right]/\Gamma(z+1), \qquad z > -1, \tag{2}$$

with r_a being the mean radius and z being a width parameter related to the polydispersity $p = (<r^2> - <r>^2)^{1/2}/<r> = (z+1)^{-1/2}$. Selected fitting results are presented in Figure S5.
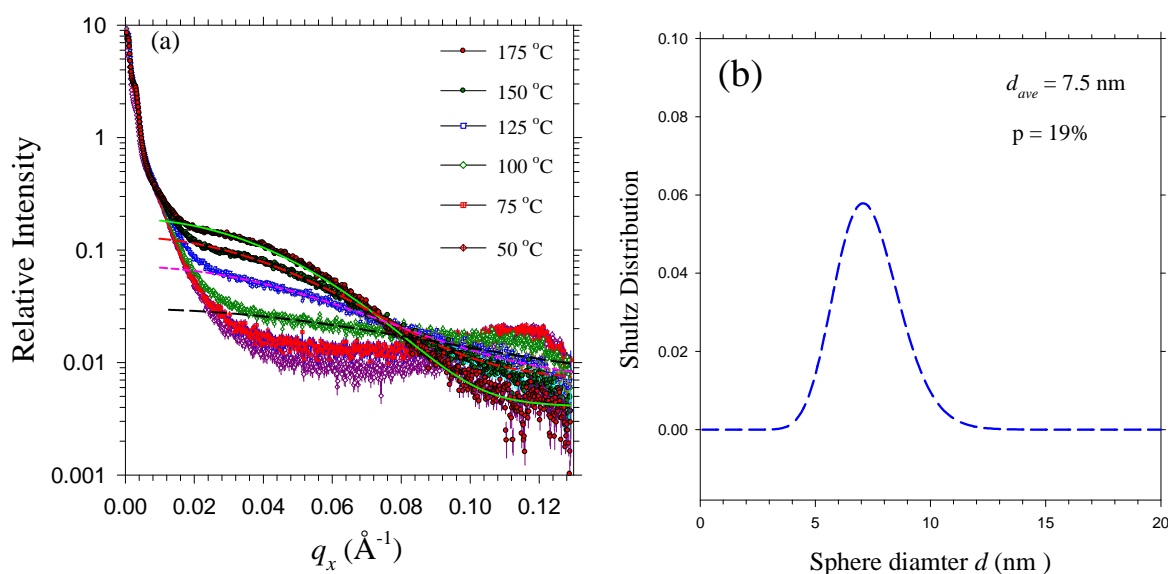
Figure S5. (a) Variable-temperature GISAXS data for the composite (DT-Ag$_{1.0}$@PS)-b-(Py-Pt$_{1.0}$@P4VP), selectively fitted (dashed curves) using a model of polydisperse spheres in the higher-q_x region. (b) Typical size distribution, with a mean diameter (d_{ave}) of 7.5 nm and a polydispersity (p) of 19%, obtained from data fitting with the GISAXS profile measured at 175 °C.
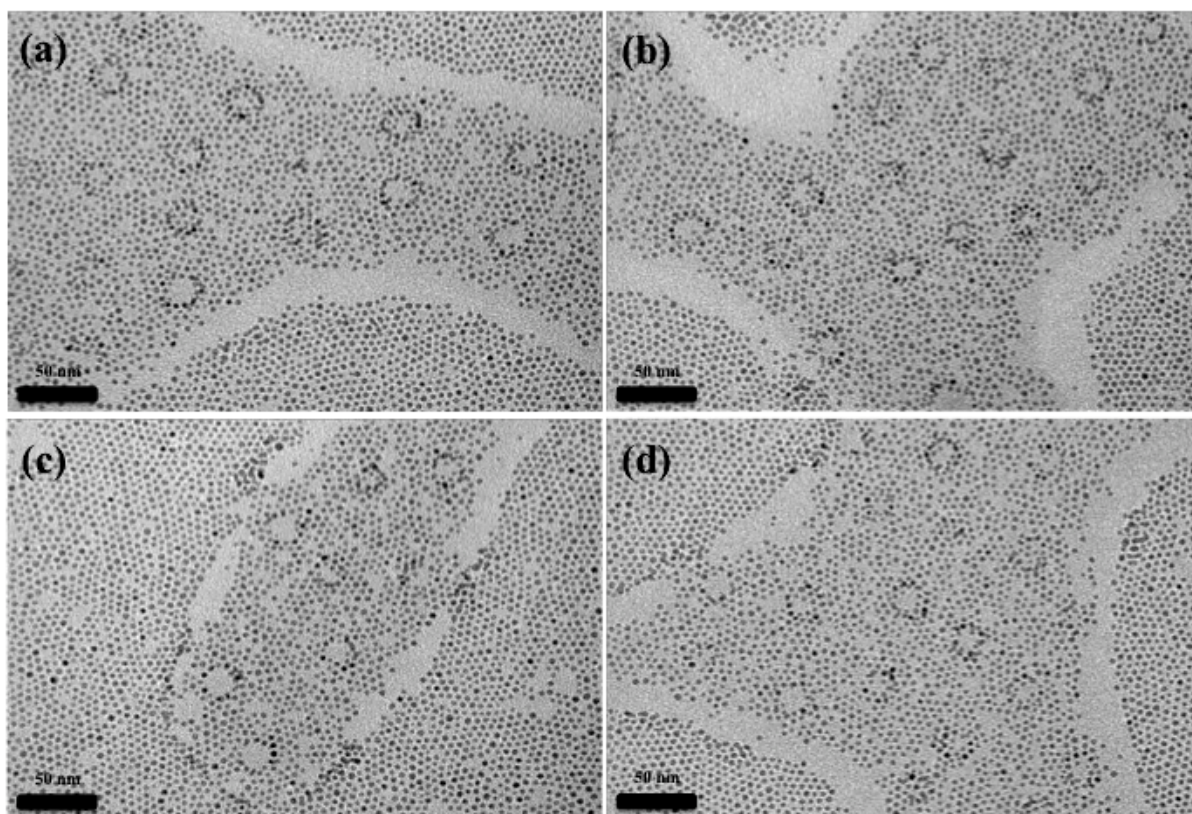
Figure S6. TEM images of (C_X-$Ag_{1.0}$@PS-*b*-P4VP) nanocomposites incorporating thiol-protected Ag NPs featuring alkyl chain lengths (X) of (a) 6, (b) 8, (c) 14, and (d) 16. From a comparison with Figure S7(b), these images indicate that all of these Ag-NPs could be embedded within the PS matrix.
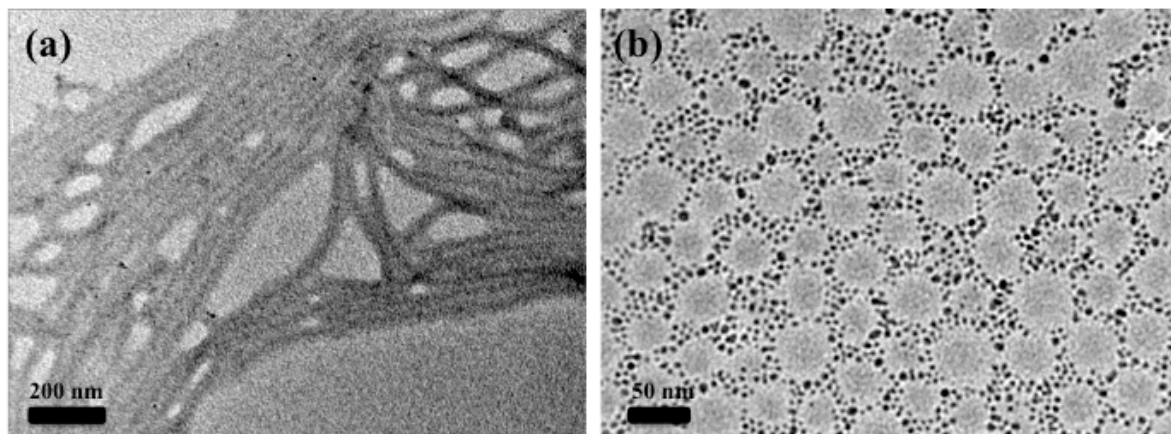
Figure S7. TEM images of (a) the cylindrical micelles of the neat copolymer PS_{48k}-*b*-$P4VP_{21k}$ (f_{PS} = 0.71) and (b) the spherical micelles of PS_{48k}-*b*-$P4VP_{21k}$ (light zones) surrounded by the DT-Ag NPs (black dots), largely segregated out from the PS phase.

References

[S1] S.-W. Yeh, K.-H. Wei, Y.-S. Sun, U. Jeng, K. S. Liang, *Macromolecules* **2003**, *36*, 7903.

[S2] S.-W. Yeh, K.-H. Wei, Y.-S. Sun, U. Jeng, K. S. Liang, *Macromolecules* **2005,** *38*, 6559.

[S3] H.-S. Sheu, U. Jeng, W.-J. Shih, Y.-H. Lai, C.-H. Su, C.-W. Lai, M.-J. Yang, Y.-C. Chen, P.-T. Chou, *J. Phys. Chem. C,* **2008**, *112*, 9617.

[S4] E. Y. Sheu, *Phys. Rev. A*, **1992**, *45*, 2428.

[S5] U. Jeng, Y.-S. Sun, H.-Y. Lee, C.-H. Hsu, K. S. Liang, S.-W. Yeh, K.-H. Wei, *Macromolecules* **2004**, *37*, 4617.

[S6] B.-H. Sohn, J.-M. Choi, I. S. Yoo, S.-H. Yun, W.-C. Zin, J. C. Jung, M. Kanehara, K. Hirata, T. Teranishi, *J. Am. Chem. Soc.* **2003**, *125*, 6368.

[S7] H. Acharya, J. Sung, B.-H. Sohn, D. H. Kim, K. Tamada, C. Park, *Chem. Mater.* **2009**, *21*, 4248.

[S8] Y.-Y. Huang, H.-L. Chen, T. Hashimoto, *Macromolecules* **2003**, *36*, 764.